



ULUSLARARASI 3B YAZICI TEKNOLOJİLERİ
VE DİJİTAL ENDÜSTRİ DERGİSİ

INTERNATIONAL JOURNAL OF 3D PRINTING
TECHNOLOGIES AND DIGITAL INDUSTRY

ISSN:2602-3350 (Online)

URL: <https://dergipark.org.tr/ij3dptdi>

A COMPUTATIONAL DETERMINATION OF A NOZZLE ACTIVATED FIXED-WING UAV

Yazarlar (Authors): Tamer Saracyakupoglu^{ID*}, Heyzem Dogukan Delibas^{ID}, Ahmet Devlet Ozcelik^{ID}




Bu makaleye şu şekilde atıfta bulunabilirsiniz (To cite to this article): Saracyakupoglu T., Delibas H. D., Ozcelik A. D., "A Computational Determination of a Nozzle Activated Fixed-Wing Uav" *Int. J. of 3D Printing Tech. Dig. Ind.*, 6(2): 292-306, (2022).

DOI: 10.46519/ij3dptdi.1128158

Araştırma Makale/ Research Article

Erişim Linki: (To link to this article): <https://dergipark.org.tr/en/pub/ij3dptdi/archive>

A COMPUTATIONAL DETERMINATION OF A NOZZLE ACTIVATED FIXED-WING UAV

Tamer Saracyakupoglu^a , Heyzem Dogukan Delibas^b , Ahmet Devlet Ozcelik^b 

^a Turkish Aerospace Industries, 06980, Ankara, TURKEY

^b Istanbul Gelisim University, Department of Aircraft Maintenance and Repair, 34315, Istanbul, TURKEY

*Correspondent Author: dr.tamer@tamersaracyakupoglu.com.tr

(Received: 09.06.2022; Revised: 26.07.2022; Accepted: 16.08.2022)

ABSTRACT

This paper proposes new methods and strategies for the propulsion of a mini Unmanned Aerial Vehicle (UAV). Typically, the UAVs are propelled by new technology batteries, fossil fuels, and hybrid systems. An experimental research regarding the usage of compressed air has been carried out. In total 13 nozzles have been installed to the fuselage of the UAV in terms of gaining 3-axis movement during flight. At the end of the manuscript, a MATLAB (Mathworks, US) program is provided in terms of calculating the maximum force and the flying time with the gained force. The UAV, whose design is presented, will be ideal for both defense and border security tasks, as it can move over the vehicle, has extremely high portability, and has a small physical footprint.

Keywords: Unmanned Aerial Vehicle (UAV), Drag, Time to Climb, Take-Off Performance, Maximum Turn Rate.

Nomenclature

W_e : Empty Weight

W_f : Fuel Weight

W_0 : Total Weight

W_e/W_0 : Empty Weight Fraction

W_f/W_0 : Fuel Fraction Weight Ratio

ρ_∞ : Density

g : Gravity

W : Total Weight

S : Wing Area

S_{ref} : Reference Area

V_{HT} : Horizontal Tail Volume Ratio

V_{VT} : Vertical Tail Volume Ratio

S_{HT} : Horizontal Tail Area

S_{VT} : Vertical Tail Area

c_{rht} : Root Chord Horizontal Tail

c_{tht} : Tip Chord Horizontal Tail

c_{rvt} : Root Chord Vertical Tail

c_{tvt} : Tip Chord Vertical Tail

y_{HT} : The Spanwise Location of the Mean Aerodynamic Chord for the Horizontal Tail

z_{HT} : The Mean Aerodynamic Chord for the Horizontal Tail

z_{VT} : The Vertical Location of the Mean Aerodynamic Chord for the Vertical Tail

c_{HT} : The Mean Aerodynamic Chord for the Vertical Tail

V_{max} : Maximum Speed

μ_∞ : Viscosity

V_{stall} : Stall Speed

b : Average span

c : Chord length

a : Speed of sound

M : Mach Number

L : Lift

D : Drag

C_L : Lift Coefficient

C_D : Drag Coefficient

C_M : Moment Coefficient

$C_{L_{max}}$: Maximum Lift Coefficient

$(L/D)_{max}$: Maximum Lift to Drag Ratio

C_{D_0} : Drag coefficient at angle of attack 0 degree

C_{D_0} : Moment coefficient at angle of attack 0 degree

AR : Aspect Ratio

λ : Taper Ratio

ρ : Air Density

T_{max} : Maximum Engine Thrust

$C.G.$: Center of Gravity

x_{cg} : Horizontal Center of Gravity

y_{cg} : Vertical Center of Gravity

x_{ac} : Aerodynamic Center

$C_{M_{aw}}$: Pitching Moment Coefficient

$C_{L_{aw}}$: Pitching Lift Coefficient

1. INTRODUCTION

The UAV that is subjected to this research study is being designed is a loiter munition UAV system. Given a specific waypoint, loiter munition can detect and destroy a moving or stationary target. The system can also work based on a certain range of fields. The UAV to be designed scans and detects the area independently and moves the target or destroys it stationary. If the target is not detected or has any plan changes, the system's rescue capability allows it to return to its base camp and land safely using a parachute and airbag. The UAV, which will be launched from a catapult, can fly for 2-3 hours by carrying a multi-sensor camera day and night. The UAV navigation system that will be built is compact and easily controlled from a personal GPS. In the open literature, some papers focus on the propelling of UAVs. Guillaume J.J. Ducard and Mike Allenspach et al [1] made investigations of designs and flight control techniques of hybrid and convertible Vertical Take-Off and Landing (VTOL) UAVs. The authors compared the three main different types of hybrid VTOL aircraft, namely 1) tail-sitters, 2) tilting-rotors, and 3) tilt-wing vehicles. This review study emphasizes that current and future movement studies development concentrate on elaborated more sophisticated approaches, both to improve model fidelity and control performance. In another study, Özgür Dündar, Mesut Bilici, and Tarık Ünler et al [2] researched the design steps and made a performance analysis regarding the energy consumption of a fixed-wing VTOL UAV. After inspection of specific Li-Po batteries installed UAV (Kuzgun), it is claimed

in this study that four propellers providing vertical take-off and landing as well as hovering increase the total drag and hence consume the battery rapidly. Conclusively the endurance is decremented. After investigating the above-mentioned scientific papers, it was observed that the above-given papers have generally concentrated on battery performance. In the open literature, the only study for the Additively Manufactured (AM) nozzle activated fixed-wing UAV was provided by Saraçyakupoğlu, T., Delibaş, H. D. and Özçelik, A. et al [3].

2. MATERIAL AND METHOD

The propulsion system is intended to use an innovative fuel, "Compressed Air". As mentioned in the introduction, the UAV is expected to fly in the air without using power on the glider principle. If there is a need for power to the UAV during the flight, it is desired to use compressed air through the nozzle. At the same time, it is aimed to realize the axis movements of the UAV with the same principle, that is, using "compressed air".

2.1. Propulsion System Working Principle

Before beginning to study the propeller system and compressed air were compared regarding the application of a novel thrust. As it is known, the rotor blades produce drag and thrust thanks to rotating airfoils. The number of the blade affects the amount of thrust directly. The thrust, torque, and demand for the power to drive the rotor will all raise as the number of blades on the rotor increases [4]. Conclusively, instead of the legacy propeller system compressed air was selected as the thrust.

As it is shown in Figure 1, the movements to be applied in 3 axes and the nozzle system to be used in the propulsion system

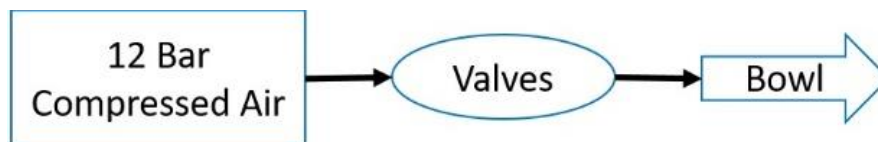


Figure 1. Propulsion System Diagram

The nozzles are positioned in the places that will give the pitch, roll, and yaw movements in the most appropriate way. In this context, positioning was carried out on the UAV as seen in Figure 2. The working principle of the nozzles has been handled in the principle of equivalence, thus providing a double-impact effect. The 3D axis movement of the UAV is expected to be provided as follows:

For the pitching movement: Nozzle 1 and Nozzle 11 & Nozzle 3 and Nozzle 9 will be operated together.

- **For the roll movement:** Nozzle 5 and Nozzle 8 & Nozzle 6 and Nozzle 7 will be operated together.

- **For yaw movement:** Nozzle 2 and Nozzle 12 & Nozzle 4 and Nozzle 10 will be operated together.

To provide thrust to the UAV: Nozzle 13 will be used.

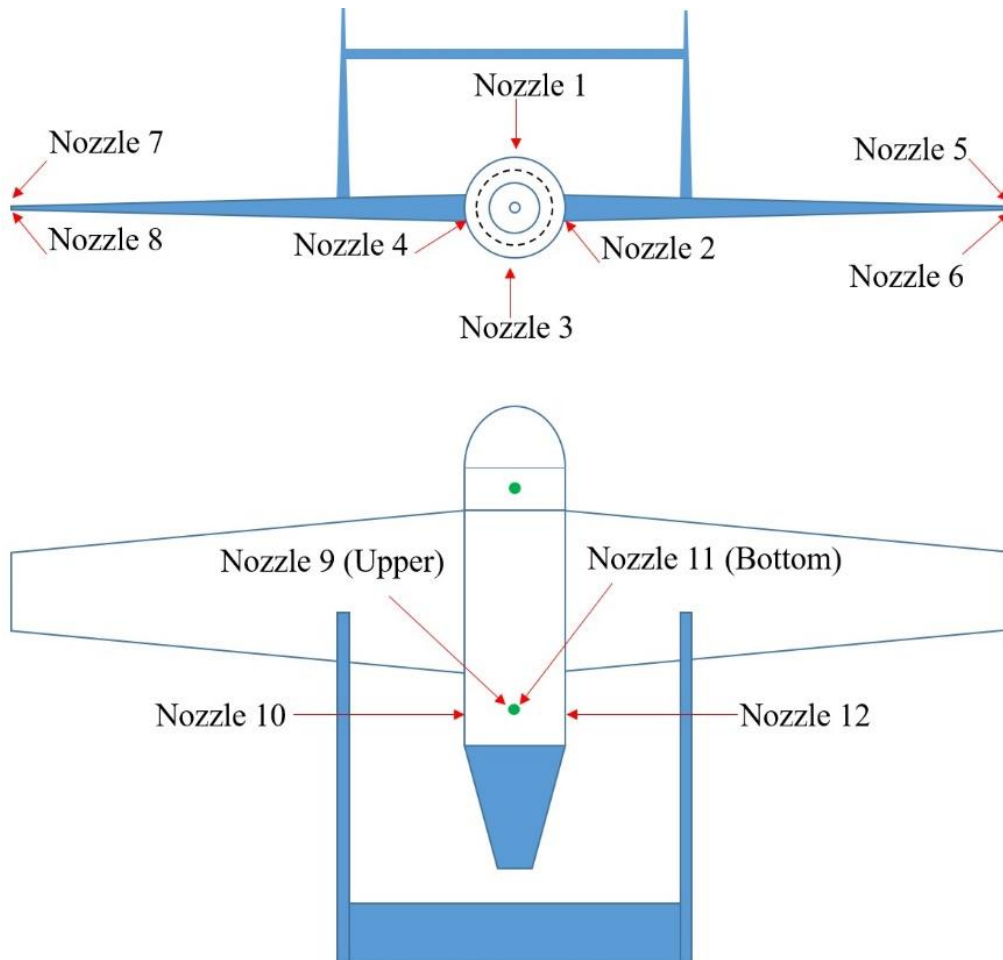


Figure 2. Placement of nozzles on the UAV

2.2. Mathematical Solution of the Propulsion System Working Principle

A system like the one above has been set up. Valves were assumed to operate at 6 bar. According to this system, the Bernoulli equation was used to find the air velocity after the valve and the exit air velocity of the nozzle. In equations (1) and (2), it was assumed that the fluid is compressible and the system is adiabatic.

$$\left(\frac{k}{k-1}\right) * \frac{P}{\rho} + \frac{V^2}{2} + g * z + \Delta h_f = C \tag{1}$$

$$\Delta h_f = f * \frac{L}{D} * \frac{V^2}{2 * g} \tag{2}$$

It was accepted that there was no height difference in the system. According to this;

$$V_2 = 3,2669 \text{ m/s}$$

$$V_3 = 7,3755 \text{ m/s}$$

By using Reynolds Transport Theorem, it is desired to find the force generated by the nozzle:

$$\frac{\delta}{\delta t} \int f dV = \int \frac{df}{dt} dV + \int (v^b \cdot n) f dA \quad (3)$$

A MATLAB code was written per the given formulas, data, and environmental conditions. The code calculates the instantaneous maximum force that the propulsion system using compressed air can give to the UAV, how long it can give this force and the moment that will occur in the axes. Code analyzes and results are given in the appendix.

Using the Reynolds Transport Theorem, the force in the nozzle was found to be 7.4102 N. The propulsion system can provide this force for 654.6 seconds (10.9 minutes). Since this force is the force that the UAV will use at stall speed, that is, at the minimum speed, less force will be applied at high speeds. When the advantage of the glider flight principle (without applying force) is combined with the time advantage this brings, the times will reach much better figures.

The force has been multiplied by the distance of the force to the axis to find the momentum that these forces will create on the axes. The nozzles on the wing are for roll motion. Taking the longitudinal axis distance of the nozzles 75 cm, the moment created here was found to be 22.4105 Nm.

The nozzles that will make the yaw movement in the body are 45 cm distance from the vertical axis, the moment created here was found to be 6.7232 Nm.

It is the same in the nozzles making the pitching movement and the moment created here was found to be 6.7232 Nm.

2.3. The Estimation of Lift And Drag Coefficients for Different Mission Configurations

This study aims to make an accurate estimation of lift and drag coefficients for different mission configurations. Stall speed, the power required for a given altitude, climb rate, maximum endurance, and maximum range are calculated according to the UAV's specifics.

2.3.1. Maximum lift coefficient

According to Raymer et al [5], it should be checked if the wing considered has a low AR or not, and taking the sweep angle of the leading edge (Λ_{LE}) equal to 0, taking $\lambda=0.45$, C_1 and C_2 are found to be 0.4 and 1 respectively. Therefore AR is calculated as given in formula (4).

$$AR \leq \frac{3}{(c_1+1)\cos\Lambda_{LE}} \quad (4)$$

AR is chosen to be 15 then the wing is considered as high AR [5]

$$C_{L_{max}} = C_{l_{max}} \left(\frac{C_{L_{max}}}{C_{l_{max}}} \right) + \Delta C_{L_{max}} \quad (5)$$

The lift coefficients' ratio is found 0.9 and Δy is found 3.12 using Δy and Λ_{LE} , $\Delta C_{L_{max}}$ is found as -0.5 [5].

From a previous study, where $C_{l_{max}}$ is the airfoil maximum lift coefficient at $M = 0.2$ with flaps; $C_{l_{max}}$ is was found as 1.2002. For a maximum speed of Mach 0.1, $\Delta C_{L_{max}}$ does not influence the $C_{L_{max}}$. The lift coefficient is finally calculated as; $C_{L_{max}} = 1.2002$

2.3.2. Drag

To calculate Parasite Drag it is solved and C_{D_0} is obtained. K value found using Equation (6). The drag value is obtained by substituting the found values in Equation. (7).

$$C_D = C_{D_0} + KC_L^2 \quad (6)$$

$$C_L = \frac{2W}{\rho_\infty V_\infty^2 S} \quad (7)$$

The C_L value changes according to the changing speed values, so the D value takes a different value according to the speed. V_∞ & D graph is obtained by using the above formula.

$$T_R = D = \frac{1}{2} \rho_\infty V_\infty^2 S C_D = \frac{1}{2} \rho_\infty V_\infty^2 S C_{D_0} + \frac{1}{2} \rho_\infty V_\infty^2 S K C_L^2 \quad (8)$$

2.4. Zero-Lift Drag and Drag due to Lift

The drag value is equal to Thrust Required (Total Drag). As a result, the V_∞ & T_R graph is obtained. As shown in Figure 3, V_∞ & Zero-Lift Drag and V_∞ & Drag due to Lift graphs are obtained, separately.

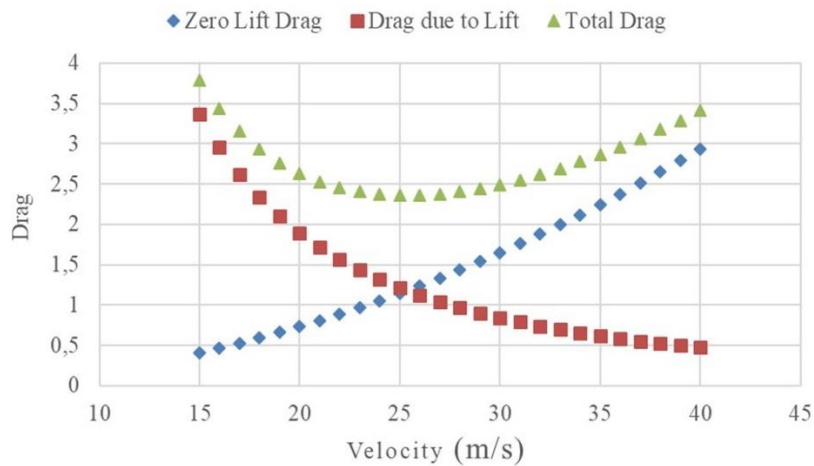


Figure 3. Drag versus velocity graph

3. EXPERIMENTAL FINDINGS

A parametric approach was introduced in the current study for reaching the followings respectively;

- Maximum Lift to Drag Ratio,
- Stall Speed,
- Required Power versus Available Power,
- Rate of Climb
- Time to Climb
- Endurance
- Range
- Take-Off Performance
- Gliding
- Level Turn
- Minimum Turn Radius

- Maximum Turn Rate
- Limiting Case for Load Factor
- Landing

3.1. Maximum Lift to Drag Ratio

The lift-to-drag ratio is one of the most important parameters affecting airplane performance. It is a direct measure of the aerodynamic efficiency of an airplane. Since C_L and C_D are both functions of the angle of attack of the airplane α , then L/D itself is a function of α .

$$T_R = \frac{W}{L/D} \tag{9}$$

As shown in Figure 4, at a peak point of L/D the velocity decrease slightly.

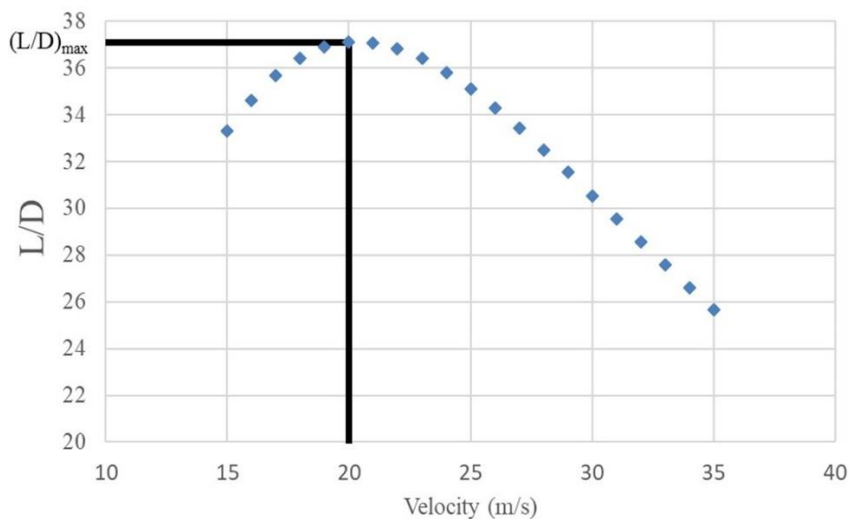


Figure 4. L/D versus velocity graph

T_R decreases as L/D increases. Indeed, minimum T_R occurs when L/D is maximum.

$$\left(\frac{L}{D}\right)_{max} = \frac{1}{\sqrt{4C_{D,0}K}} = 37.11 \quad (10)$$

3.2. Stall Speed

The stall speed is an important parameter for the UAV characteristics V_{stall} is calculated according to H.Y.Akdeniz et al [6] using the density of air at sea level, wing loading is already known from previous studies and maximum lift coefficient is found in this study. V_{stall} is calculated 14.79 m/s as given in (11)

$$V_{stall} = \sqrt{\frac{2W}{\rho S C_{Lmax}}} = 14.79 \text{ m/s} \quad (11)$$

3.3. Power Required versus Power Available Curves and Maximum Velocity

For a subsonic UAV, the power available is essentially constant with velocity. The high-speed intersection of the maximum power available curve and the power required curve defines the maximum velocity of the airplane.

In steady flight, equating thrust to drag and multiplying it with velocity results in the power required value for each different velocity. Power available is found by multiplying engine power with engine efficiency. Power available defines the maximum velocity the aircraft can achieve. According to Anderson et al [7] Figure 5 shows that;

$$V_{\infty max} = 37 \text{ m/s (133.2 km/h)}$$

$$P_A = 112.05 \text{ W}$$

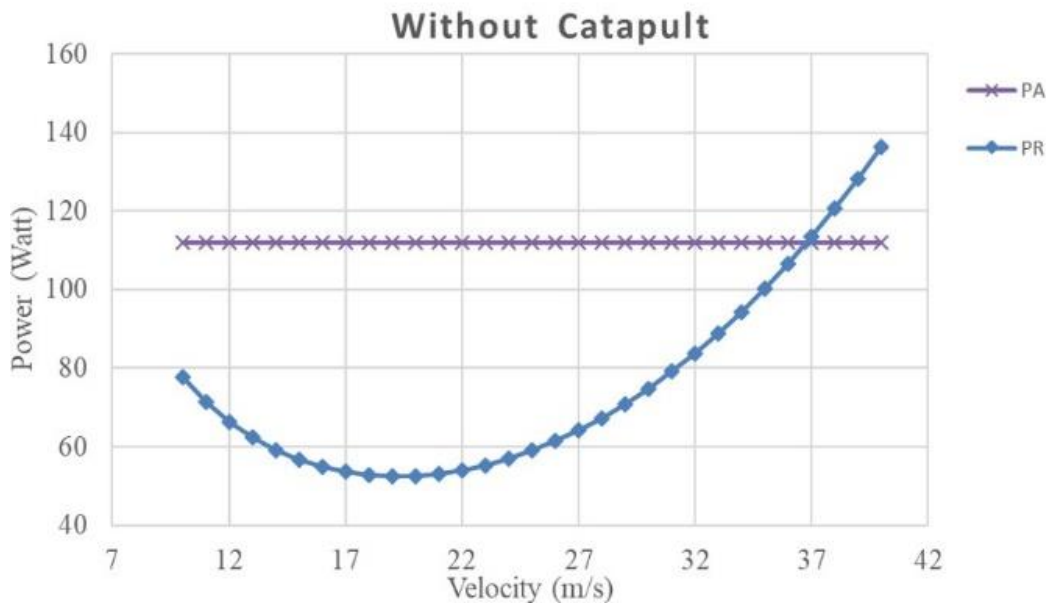


Figure 5. Power required versus power available and maximum velocity

3.4. Rate of Climb

According to Saracyakupoglu et al [8] weight dominates the performance of a flight. The rate of climb is the difference between the power available and the power required divided by weight. It represents the upward climb rate of the UAV. The rate of climb will be calculated using the previously obtained values. According to the information learned from the company, the power of the catapult selected for the UAV is 14 kW. The power obtained without

the catapult is only 110 W. The Rate of Climb value will be calculated in two possibilities, with and without the help of catapults.

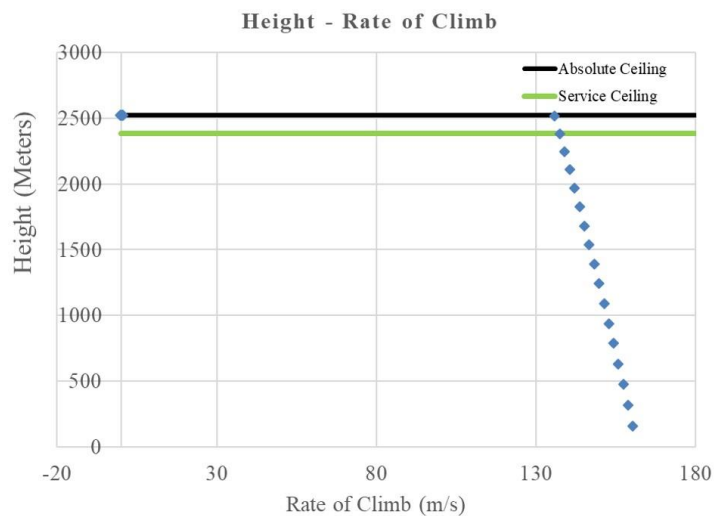
$$\frac{R}{C} = V_{\infty} \sin\theta = \frac{TV_{\infty} - DV_{\infty}}{W} \quad (12)$$

R/C values are calculated for different altitudes and the results are shown in Table 1. The rate of climb decreases with increasing altitude because the air density goes lower as altitude increases.

Table 1. R/C and altitude differences

Rate of Climb R/C	Rate of Climb R/C with Catapult	Altitude (m)
0,393079223	160,3199972	160,3199972
0,464866391	158,8496319	319,1696291
0,522150081	157,3647632	476,5343923
0,567832375	155,8682931	632,4026854
0,603950268	154,3622585	786,7649439
0,631964029	152,8481199	939,6130638
0,65293743	151,3269409	1090,940005
0,66765436	149,7995054	1240,73951
0,676696572	148,2663952	1389,005905
0,680496875	146,728043	1535,733948
0,679376373	145,1847701	1680,918718
0,673571058	143,6368124	1824,555531
0,663251157	142,08434	1966,639871
0,648535426	140,5274719	2107,167343
0,629501873	138,9662859	2246,133629
0,606195912	137,4008275	2383,534456
0,578636624	135,8311158	2519,365572
0,54682164	0,54682164	2519,912394
0,510730968	0,510730968	2520,423125
0,470330031	0,470330031	2520,893455
0,425572101	0,425572101	2521,319027
0,376400254	0,376400254	2521,695427
0,322748969	0,322748969	2522,018176
0,264545425	0,264545425	2522,282721
0,201710578	0,201710578	2522,484432
0,134160049	0,134160049	2522,618592
0,061804865	0,061804865	2522,680397
-0,015447921	-0,015447921	2522,664949
-0,097694704	-0,097694704	2522,567254
-0,18503489	-0,18503489	2522,382219
-0,277570515	-0,277570515	2522,104649

Per Table 1, the service and absolute ceiling are provided in Figure 6.

**Figure 6.** Service and absolute ceiling

Thanks to the catapult, the UAV can easily achieve the desired power while ascending to altitude. Service Ceiling is the height obtained when the Rate of Climb speed reaches 25 m/s, that is, cruising speed. The Service Ceiling value, which corresponds to 25 m/s thus obtained, is 2383 m.

R/C values turn negative after 36 m/s in Rate of Climb values calculated without the aid of catapults, and the climb ends. For this reason, in the Rate of Climb values calculated by including the catapult aid, the height reached when the UAV speed is 36 m/s is the maximum height that the UAV can reach, that is, Absolute Ceiling. According to all these, the Absolute Ceiling value is 2522 m.

While all these calculations, tables, and graphics were obtained, the speed value was passed to the rate of climb value and then to the altitude value.

For weight reduction, as an alternative material, Carbon Fiber Reinforced Polymer (CFRP) is widely used for manufacturing UAVs [9, 10].

3.5. Time to Climb

Normally, the performance characteristic labeled time to climb is considered from sea level. Hence, the time to climb from sea level to any given altitude Absolute Ceiling is given in formula (13) [11].

$$t = \int_0^{h_2} \frac{dh}{R/C} \quad (13)$$

The absolute ceiling is the altitude at which the (maximum) rate of the climb goes to zero.

According to the calculations, the UAV climbs the service ceiling in 16 seconds. The same UAV reaches the absolute ceiling in 23 seconds.

$$t_{service\ ceiling} = 16\ s \quad (14)$$

$$t_{absolute\ ceiling} = 23\ s \quad (15)$$

3.6. Endurance

Fuel-drinking air-breathing engines are not the answer to the ever-increasing demand for flying time. An aircraft's endurance must meet the mission requirement, which can be;

a. A few hours such as broadcasting a concert or sports event,

b. A few days such as border surveillance, Search and Rescue (SAR) Operations,

c. A few months such as continuous air surveillance, communication relay, and meteorological investigations [12].

To reach the endurance value, it is necessary to examine the propulsion system closely. As stated in the code written on the propulsion system, the propulsion system can provide 7.47N thrust to the UAV for 11 minutes. The multiplication of these two values gives 110.48 W, which is the constant Power value of the propulsion system. The UAV, which will be brought to cruising speed (25 m/s) with the help of the catapult, will apply a force of 4.42 at that speed. At this force, the propulsion system can provide continuous thrust for 18.44 minutes. In addition, since it will fly without using propulsion with the glider principle while performing its flight, the time to stay in the air has been determined as 18<.

$$E_{without\ gliding} = 18\ min < \quad (16)$$

Despite the values found, it is estimated that the UAV can stay in the air for about 1 hour depending on the flight missions.

3.7. Range

The range value will be obtained by including the calculations while finding the endurance value. It has been determined that the UAV will have a range of 27 km (27000 m) by providing 18 minutes of flight at cruising speed (25 m/s). It can also be said that it has a range exceeding 50 km, assuming that it will fly at maximum flight speed, faster and longer, and will go further without applying thrust with the glider principle.

$$R_{without\ gliding} = 27\ km < \quad (17)$$

Despite the values found, it is estimated that the UAV will have a range of close to 50 km depending on its flight missions.

3.8. Take-Off Performance

It is decided to launch the UAV with a catapult to make it easier to hold in the air. The use of a UAV catapult reduces the need for a take-off path [13]. This is especially important in battle situations where the runway's availability is unpredictable. It is deemed appropriate to

launch with an initial velocity of 25 m/s at an angle of 11 degrees. It is envisaged to design or purchase a catapult that provided the required features.

The power that the selected catapult can provide to the UAV is 14 kW. More than enough for the desired speed and altitude in the UAV.

It is decided to integrate this found force data into the following performance parameters:

- Power Available
- Rate of Climb
- Time to Climb
- Service and Absolute Ceilings

3.9. Gliding

Gliding is one of the most important features of an air vehicle. Depending on the meteorological conditions glide ratio may differ from 1:30 to 1:70 [14]. In the case of the glider principle, the UAV does the gliding (unpowered) flight, the UAV will descend rather than climb. For the UAV at a given altitude of 2383 m taking the $(L/D)_{max} = 37.11$, the glide angle can be found by Eq.

$$\tan\theta_{min} = \frac{1}{(L/D)_{max}} \tag{18}$$

$$\theta_{min} = 1.55 \text{ deg} \tag{19}$$

The equilibrium glide angle does not depend on altitude or wing loading, it simply depends on the lift-to-drag ratio. However, to achieve the given L/D at a given altitude, the UAV must fly at a specified velocity called the equilibrium glide velocity and it can be found as;

$$V_{\infty} = \sqrt{\frac{2\cos\theta W}{\rho_{\infty} C_L S}} \tag{20}$$

The UAV starts gliding at mid-cruise speed (25 m/s), taking $\rho_{\infty} = 0.9578 \text{ kg.m}^{-3}$ at 2383 m, $W = 8.92 \text{ kg}$, $S = 0.6 \text{ m}^2$ and $C_{Lmax} = 1.2$, V_{∞} can be found as 15.93 m/s. The aircraft achieves the equilibrium glide velocity. Assuming the L/D variable as constant and the gliding path straight the range covered in an equilibrium glide is shown in Figure 7.

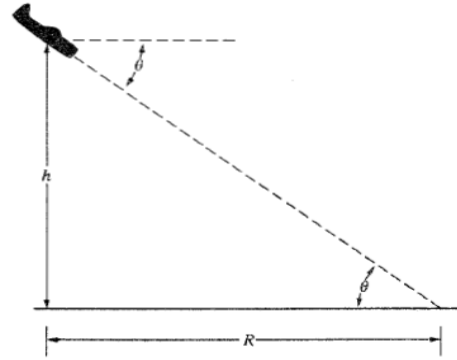


Figure 7. Range covered in an equilibrium glide

The distance can be found by multiplying altitude (h) with the L/D ratio. Altitude is 2383 m and L/D is taken as 37.11, the total distance aircraft will cover after the engine failure is;

$$R = 88.1 \text{ km.} \tag{21}$$

This study is going to cover the topic of UAV maneuverability. Accelerated flight in level turn is studied meaning the altitude will stay constant.

3.10. Level Turn

During the level turn, the UAV's altitude stays constant. The turn performance is affected by the UAV's load factor (n) and it is found by dividing UAV's lift by its weight. The load factor value is dependent on UAV's velocity, for each different velocity, a different n_{max} value can be calculated as given in (22).

$$n_{max} = \left\{ \frac{\frac{1}{2}\rho_{\infty}V_{\infty}^2}{K\left(\frac{W}{S}\right)} \left[\left(\frac{P}{VW}\right)_{max} - \frac{1}{2}\rho_{\infty}V_{\infty}^2 \frac{C_{D,0}}{W/S} \right] \right\}^{1/2} \tag{22}$$

For velocities below the stall speed, the above equation cannot be used because the aircraft's maximum lift coefficient $((C_L)_{max})$ value constraints the equation. For velocities below the stall speed, can be used as given in formula (23).

$$n_{max} = \frac{1}{2}\rho_{\infty}V_{\infty} \frac{(C_L)_{max}}{W/S} \tag{23}$$

Bank angle depends only on the load factor, which can be calculated as provided in formula (24).

$$\phi = \text{Arccos} \frac{1}{n} \tag{24}$$

According to calculations in (22), (23), and (24) the velocity versus load factor and the velocity versus bank angle are provided in Figure 8 and Figure 9 respectively.

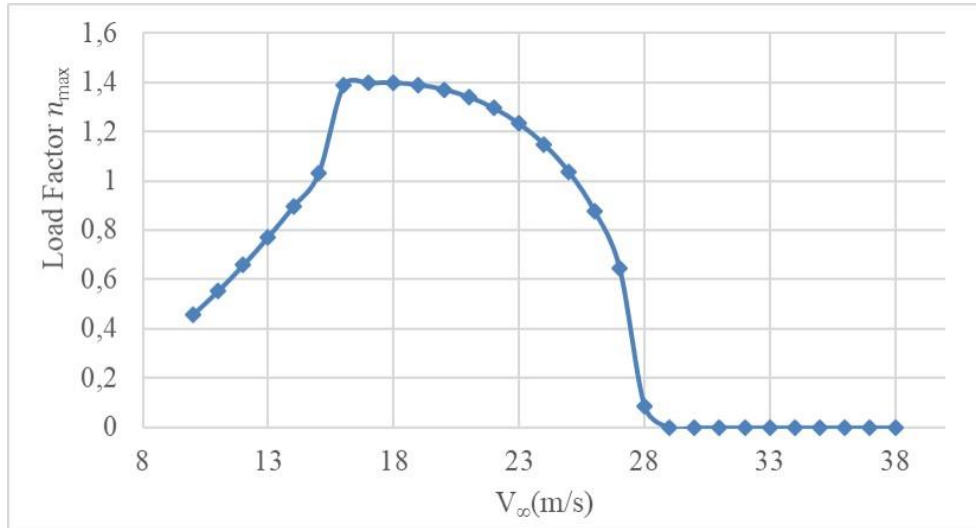


Figure 8. Velocity versus Load Factor

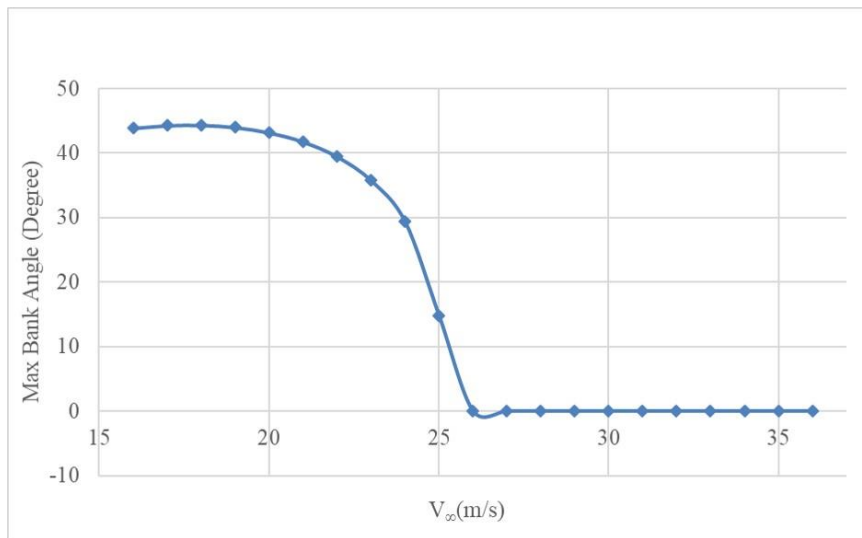


Figure 9. Velocity versus Bank Angle

3.11. Minimum Turn Radius

Minimum turn radius is the performance parameter that defines its minimum radius in the same level turn. The lower turn radius is more desirable for UAVs. In general, low velocities have less minimum turn radius but it should not be lower than stall speed. Once again, instead of thrust, power is used. Equation (6.31) gives the value of V_∞ which corresponds to the minimum turning radius;

$$(V_\infty)_{R_{min}} = \sqrt{\frac{4K(\frac{W}{S})}{\rho_\infty(\frac{T}{W})}} \quad (25)$$

Equation (6.32) gives the load factor corresponding to the minimum turning radius;

$$n_{R_{min}} = \sqrt{2 - \frac{4KC_{D,0}}{(\frac{T}{W})^2}} \quad (26)$$

The general equation for minimum turn radius power is changed as provided in formula (27);

$$R_{min} = \frac{4K(\frac{W}{S})}{g\rho_\infty(\frac{P}{W})\sqrt{1 - \frac{4KC_{D,0}}{(\frac{P}{W})^2}}} \quad (27)$$

At sea level, R_{min} is found 21.80 m. It should be checked if the corresponding velocity is lower than stall speed or not. The general equation for corresponding velocity and corresponding load factor is respectively described below;

The corresponding velocity for the minimum turn radius is found as 14.25 m/s. The UAV's

stall speed is 14.71 m/s, so it is not acceptable. When R_{min} is recalculated according to stall speed, the value found is 21.89 m.

The corresponding maximum load factor for minimum turn radius is found as 1.38.

3.12. Maximum Turn Rate

The process for finding the maximum turn rate is similar to the turn radius. Higher maximum turn rates are desirable for UAVs. Once again, the lower speeds correspond to higher maximum turn rates, but it should be checked that velocity should not be lower than stall speed. Instead of thrust, power is used as the given formula (28).

$$(V_{\infty})_{\omega_{max}} = \left[\frac{2(\frac{W}{S})}{\rho_{\infty}} \right]^{1/2} \left(\frac{K}{C_{D,0}} \right)^{1/4} \tag{28}$$

$$n_{\omega_{max}} = \left(\frac{T/W}{\sqrt{4KC_{D,0}}} - 1 \right)^{1/2} \tag{29}$$

$$\omega_{max} = q \sqrt{\frac{\rho_{\infty}}{(\frac{W}{S})} \left[\frac{(\frac{P}{VW})}{2K} - \left(\frac{C_{D,0}}{K} \right)^{1/2} \right]} \tag{30}$$

The maximum turn rate is found 29.89 deg/s. It should be checked if the corresponding velocity is lower than stall speed or not. Corresponding

velocity and corresponding load factor can be calculated from equations (29) and (30) respectively.

The corresponding velocity for maximum turn rate is found as 25.35 m/s, it is higher than the UAV's stall speed so it's acceptable. The corresponding load factor is found as 2.31.

3.13. Limiting Case for Load Factor

The load factor can be defined as the ratio of the lift of an aircraft to its weight and represents a global measure of the stress ("load") to which the structure of the air vehicle. The maximum load factor permissible for a given UAV is constrained by structural constraints. The boundary associated with persistent structural deformation of one or more components of the UAV is known as the limit load factor. The structure may reflect during a maneuver if the load factor is less than the limit load factor, but it will return to its original state when $n=1$. If n is more than the limit load factor, the UAV structure will suffer permanent deformation, resulting in structural damage. The ultimate load factor is the point at which a structure will fail completely. If n exceeds the ultimate load factor, pieces of the UAV will be damaged. break.

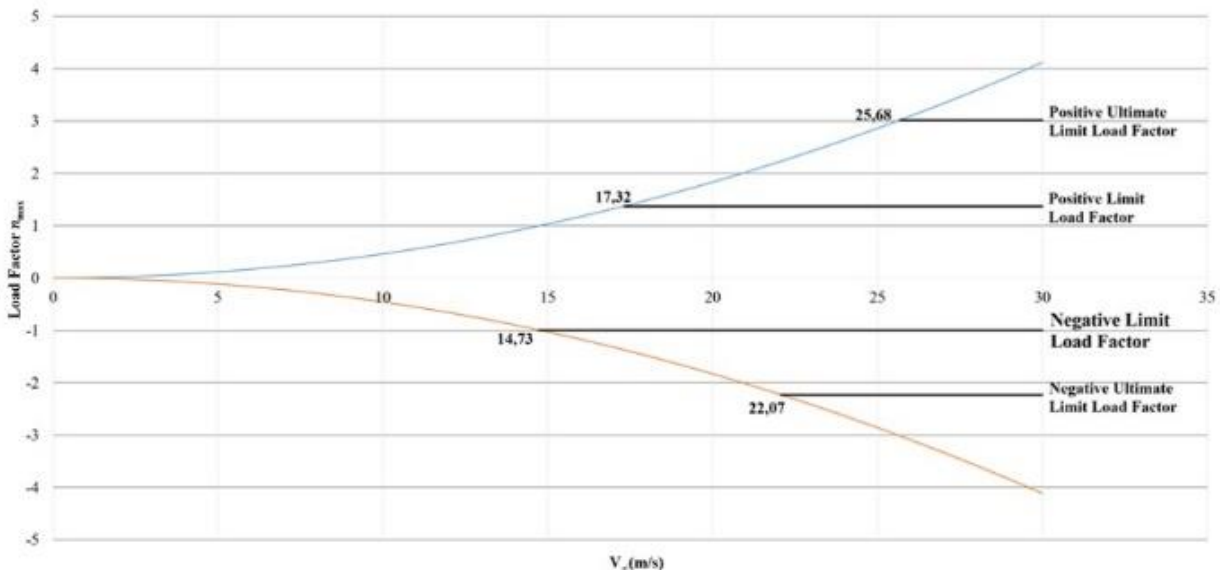


Figure 10. Velocity versus load factor diagram

In Figure 10, both curves are plotted with aerodynamic limitation maximum lift coefficient ($(C_L)_{max}$). The left side of curves is stall regions where it is unobtainable in flight. The cornering velocity is the corresponding velocity to the positive limit load factor and is represented as V^* in Figure 10 and is found as formula (31).

$$V^* = \sqrt{\frac{n_{max} W}{\rho_{\infty} (C_L)_{max} S}} = 17.12 \text{ m/s} \quad (31)$$

Density at sea level is used to find the corner velocity. At velocities higher than V^* the UAV must fly at values of C_L less than $(C_L)_{max}$ so that the positive limit load factor is not exceeded if it is exceeded then structural damage or possibly structural failure will occur. The right-hand side of Figure 10 is the maximum cruise speed limit where already the aircraft cannot exceed. It is mostly defined by the engine's power. The bottom side of the graph corresponds to a negative angle of attack hence negative $(C_L)_{max}$ and negative limit load factor. The positive side of the graph's limitations is also valid for the negative side. Ultimate load factors are found by multiplying limit load factors by 1.5 which is a generic method.

3.14. Landing

In a regular flight, the landing is the most important phase in terms of flight safety. The landing gear is an assembly that has many sub-assemblies which are subject to one of the most critical systems of an aircraft [15]. 20% of aircraft accidents happen during the landing stage of a flight [16]. Landing gear collapses and hard landing are the most common type of incidents that happen during the landing phase [17]. In reality, the landing gear of a UAV is the most important piece of equipment for the vehicle to land securely on uneven ground. There are significant researches regarding the energy consumption and sustainability rates of UAVs [18]. It is noteworthy that at present, the research about dynamic and adaptive landing gear for UAVs has increased since it provides many advantages [19]. In this study, a smooth landing with a shallow approach angle was assumed.

4. RESULTS AND CONCLUSIONS

In this paper, the conceptual design of a loitering munition is discussed. Starting from the idea stage, UAV performance values were

calculated. Although the numerical values calculated in this study are consistent; analysis and software programs were also used. With the help of the MATLAB program provided in the appendix paragraph, the three main requirements can be easily calculated. These requirements are given below;

- a. The Maximum Force (N),
- b. Maximum Flying Time (Min),
- c. The compressed air flowing time while the valves are fully open (Min).

In the first stage, the propulsion system working with the compressed air tank was designed and the power it would give was calculated. All the desired performance values of the UAV, which was designed in the Result section and whose propulsion system was integrated, were calculated. Finally, maneuvering and load exposure conditions after the UAV, which meets all the desired performance requirements, were calculated and analyzed.

Also, originally a compressed air tank was used as a propulsion system in this paper. The UAV, which will also benefit from the glider principle due to its design features, foresees a serious energy-saving and therefore environmentally friendly design, both with its propulsion system and by traveling long distances without power. Apart from this, the UAV, which will perform the axis movements not with the moving parts, but with the valves working with the compressed air tank, will have another unique feature.

As another feature, the conceptual design of the UAV will be used in kamikaze missions. It is expected to focus on the target it has determined and destroy that target. Due to this feature, the design requirements will be optimized so that the production is simple and the cost is cheap.

In the next stage, it is recommended to carry out test flights of the original production, if the design is implemented in real life, the prototype is put into tests and then successfully passed.

APPENDIX

```
clc
```

```
clear all
```

```
%Air @1000 m
```

```
P_air_outside=8.988*10^4; %N/m^2
```

```

T_air_outside=8.5; %C
rho_air_outside=AirProperties(T_air_outside,
P_air_outside/100, 1, 'rho'); %kg/m^3
mu_air_outside=AirProperties(T_air_outside,
P_air_outside/100, 1, 'mu'); %N*s/m^2
k_air_outside=AirProperties(T_air_outside,
P_air_outside/100, 1, 'k'); %W/m*K

% Air @ 1.2 Mpa

P_air_pressurized_1=1200000; %N/m^2
T_air_pressurized_1=8.5; %C
rho_air_pressurized_1=AirProperties(T_air_pr
essurized_1, P_air_pressurized_1/100, 1, 'rho');
%kg/m^3
mu_air_pressurized_1=AirProperties(T_air_pr
essurized_1, P_air_pressurized_1/100, 1, 'mu');
%N*s/m^2
k_air_pressurized_1=AirProperties(T_air_pres
surized_1, P_air_pressurized_1/100, 1, 'k');
%W/m*K
% Air @ 0.6 Mpa

P_air_pressurized_2=600000; %N/m^2
T_air_pressurized_2=8.5; %C
rho_air_pressurized_2=AirProperties(T_air_pr
essurized_2, P_air_pressurized_2/100, 1, 'rho');
%kg/m^3
mu_air_pressurized_2=AirProperties(T_air_pr
essurized_2, P_air_pressurized_2/100, 1, 'mu');
%N*s/m^2
k_air_pressurized_2=AirProperties(T_air_pres
surized_2, P_air_pressurized_2/100, 1, 'k');
%W/m*K
%Other Inputs

d_pipe=0.004; %m
d_nozzle=0.001; %m

roughness_pipe=3.334*10^-6; %m
L=0.75; %m

%Let's start then! Adiabatic Compressible
Flow!

%First calculate the V_2!!

Section_1=(k_air_pressurized_1/(k_air_pressu
rized_1-
1))*(P_air_pressurized_1/rho_air_pressurized_
1);
Section_2_P=(k_air_pressurized_2/(k_air_pres
surized_2-

```

```

1))*(P_air_pressurized_2/rho_air_pressurized_
2);
V_2=sqrt((Section_1-Section_2_P)*2);

%Let's calculate Reynolds and Relative
Roughness

Re=rho_air_pressurized_2*V_2*d_pipe/mu_ai
r_pressurized_2;
K=roughness_pipe/d_pipe;
f=colebrook(Re,K);
delta_h=f*(L/d_pipe)*(V_2^2)/(2*9.81);
% V_3

Section_2=(k_air_pressurized_2/(k_air_pressu
rized_2-
1))*(P_air_pressurized_2/rho_air_pressurized_
2)+(V_2^2)/2;
Section_3=(k_air_outside/(k_air_outside-
1))*(P_air_outside/rho_air_outside)+9.81*delt
a_h;

V_3=sqrt(abs(Section_2-Section_3)*2); %m/s

%Now using Reynolds Transport Theorem we
can calculate the forces that
%happened because of pressurized air

A_nozzle=pi*((d_nozzle/2)^2);
A_pipe=pi*((d_pipe/2)^2);

%Forces due to Pressure

F_2_P=-P_air_pressurized_2*A_pipe;
F_3_P=P_air_outside*A_nozzle;

%Forces due to Velocity

F_2_V=-
rho_air_pressurized_2*V_2*V_2*A_pipe;
F_3_V=rho_air_outside*V_3*V_3*A_nozzle;

sum_of_forces=F_2_P+F_3_P+F_2_V+F_3_V
%N

%Momentum that will be used for roll

M_roll=sum_of_forces*1.5*2 %N*m

%Momentum that will be used for pitch

M_pitch=sum_of_forces*0.45*2 %N*m

%Momentum that will be used for pitch

```

$$M_{yaw} = \text{sum_of_forces} * 0.45 * 2 \% N * m$$

$$m_{dot} = \rho_{air} * \text{pressurized_2} * A_{pipe} * V_2;$$

$$\text{air_time} = 0.2 / m_{dot}$$

ACKNOWLEDGES

The support that is provided by Istanbul Gelisim University is gratefully acknowledged. The authors also appreciate the helpful and constructive comments of the valuable reviewers.

CONFLICT OF INTEREST

The authors state that they have no known competing financial interests or personnel connections that could have influenced the research presented in this study.

REFERENCES

1. Ducard, J.J.G., Allenspach, M., "Review of designs and flight control techniques of hybrid and convertible VTOL UAVs", *Aerospace Science and Technology*, Volume 118, Pages 1-25, 2021.
2. Dündar, Ö., Bilici, M., Ünler, T., "Design and performance analyses of a fixed wing battery VTOL UAV", *Engineering Science and Technology, an International Journal*, Volume 23, Issue 5, Pages 1-12, 2020.
3. Saraçyakupoğlu, T. , Delibaş, H. D. , Özçelik, A. D. "An Experimental Determination and Numerical Analysis Of A Loiter Munition Unmanned Aerial Vehicle System". *International Journal of 3D Printing Technologies and Digital Industry*, Volume 6, Issue 1, Pages 83-101, 2022.
4. Göv, İ., "Rotor Spacing and Blade Number Effect on the Thrust, Torque and Power of a Coaxial Rotor", *El-Cezeri Journal of Science and Engineering*, Volume 7, Pages 487-502, 2020.
5. Raymer, D. P., "Aircraft Design: A Conceptual Approach", *American Institute of Aeronautics and Astronautics-AIAA*, Page 273, 1992.
6. Akdeniz, H. Y., "A Study on Aerodynamic Behavior of Subsonic UAVs' Wing Sections with Flaps", *International Journal of Aviation Science and Technology*, Volume 02, Issue 01, Pages 22-27, 2021.

7. Anderson, J. D., "Aircraft Performance and Design", WCB/McGraw-Hill. Boston, Page 453, 1999.
8. Saraçyakupoğlu, T., "The Qualification of the Additively Manufactured Parts in the Aviation Industry", *American Journal of Aerospace Engineering*, Volume 6, Issue 1, Pages 1-10, 2019.
9. Saraçyakupoğlu, T. "Abrasive Water Jet (AWJ) Applications in the Aviation Industry", *International Journal of Mechanical and Production Engineering Research and Development (IJMPERD)*, Volume 9, Issue 6, Pages 347-356, 2019.
10. Saraçyakupoğlu, T., "Emniyet İrtifasından Bilgiler: Genel Havacılık, Üretim ve Bakım Süreçleri". ISBN: 978-625-402-030-8, Nobel Academic Publishing, Ankara, Page 55, 2020.
11. Gudmunsson, S., "General Aviation Aircraft Design: Applied Methods and Procedures", Elsevier, Oxford, Page 21, 2014.
12. Bakar, A., Ke, L., Liu, H., Xu, Z., Wen, D., "Design of Low Altitude Long Endurance Solar-Powered UAV Using Genetic Algorithm", *Aerospace*, Volume 8, Issue 228, Pages 1-24, 2021.
13. Novaković, Z., Vasić, Z., Ilić, I., Medar, N., Stevanović, D., "Integration of Tactical - Medium Range UAV and Catapult Launch System", *Scientific Technical Review*, Volume 66, Issue 4, Pages 22-28, 2016.
14. Keskin, G., Durmuş, S., Karakaya, M., Teoman, A., Kuşhan, M. C., "Unpowered Flight Principle: Sailplane", *Engineer and the Machinery Magazine*, Volume 60, Issue 695, Pages 165-177, 2019.
15. Saraçyakupoğlu, T., "3D Manufacturing Applications in Aviation Industry in Accordance with the Airworthiness Rules And Regulations: A Review". *International Journal of 3D Printing Technologies and Digital Industry*, Volume 4, Issue 1, Pages 53-65, 2020.
16. Saraçyakupoğlu, T., "Havacılıkta organizasyonel kazalar: B-737 max uçak kazalarının mühendislik perspektifinden incelenmesi ", *Mühendis ve Makina*, Vol. 61, Issue 701, Pages 241-261, 2020.

17. Saracyakupoğlu, T., “The Adverse Effects of Implementation of the Novel Systems in the Aviation Industry in Pursuit of Maneuvering Characteristics Augmentation System (MCAS)”. *Journal of Critical Reviews*, Volume 7, Issue 11, Pages 2530-2538, 2020.

18. Balli, O., Caliskan, H., "On-design and off-design operation performance assessments of an aero turboprop engine used on unmanned aerial vehicles (UAVs) in terms of aviation, thermodynamic, environmental and sustainability perspectives", *Energy Conversion and Management*, Vol 243, Pages 1-13, 2021.

19. Çabuk, N., “Design and Kinematic Analysis of Proposed Adaptive Landing Gear for Multirotor UAV”, *El-Cezerî Journal of Science and Engineering*, Volume 9, Issue 1, Pages 159-170, 2022.